HHS Public Access

Author manuscript

Bioconjug Chem. Author manuscript; available in PMC 2021 April 15.

Published in final edited form as:

Bioconjug Chem. 2018 November 21; 29(11): 3768–3775. doi:10.1021/acs.bioconjchem.8b00639.

A Mechanistic Investigation of Methylene Blue and Heparin Interactions and Their Photoacoustic Enhancement

Junxin Wang[#†], **Ananthakrishnan Soundaram Jeevarathinam**[#†], **Kathryn Humphries**[‡], **Anamik Jhunjhunwala**[‖], **Fang Chen**[†,§], **Ali Hariri**[†], **Bill R. Miller III**[‡], **Jesse V. Jokerst**[*,†,§,⊥]

[†]Department of NanoEngineering, University of California, San Diego, 9500 Gilman Drive, La Jolla, California 92093, United States

[§]Materials Science and Engineering Program, University of California, San Diego, 9500 Gilman Drive, La Jolla, California 92093, United States

[‖]Department of BioEngineering, University of California, San Diego, 9500 Gilman Drive, La Jolla, California 92093, United States

[⊥]Department of Radiology, University of California, San Diego, 9500 Gilman Drive, La Jolla, California 92093, United States

[‡]Department of Chemistry, Truman State University, 100 East Normal Avenue, Kirksville, Missouri 63501, United States

[#] These authors contributed equally to this work.

Abstract

We recently reported a real-time method to measure heparin in human whole blood based on the photoacoustic change of methylene blue (MB). Intriguingly, the MB behaved unlike other “turn on” photoacoustic probes—the absorbance decreased as the photoacoustic signal increased. The underlying mechanism was not clear and motivated this study. We studied the binding mechanism of MB and heparin in water and phosphate buffer saline (PBS) with both experimental and computational methods. We found that the photoacoustic enhancement of the MB–heparin mixture was a result of MB–heparin aggregation due to charge neutralization and resulting sequestration of MB in these aggregates. The sequestration of MB in the MB–heparin aggregates led to decreased absorbance—there was simply less free dye in solution to absorb light. The highest photoacoustic signal and aggregation occurred when the number of negatively charged sulfate groups on heparin was approximately equal to the number of positively charged MB molecule. The MB–heparin aggregates dissociated when there were more sulfated groups from heparin than MB molecules because of the electrostatic repulsion between negatively charged sulfate groups. PBS facilitated

[*]**Corresponding Author** jjokerst@ucsd.edu.

Supporting Information

The Supporting Information is available free of charge on the ACS Publications website at DOI: 10.1021/acs.bioconjchem.8b00639.

Chemical structure of heparin and heparin:MB ratio; size of MB–heparin aggregates; NMR spectrum of MB–heparin complex; PBS effect in MB–heparin binding (PDF)

Binding dynamics of MB and heparin in 0.154 M NaCl (MPG)

Binding dynamics of MB and heparin in 1X PBS (MPG)

The authors declare no competing financial interest.

MB dimer formation regardless of heparin concentration and reprecipitated free MB in aggregates due to ionic strength and ionic shielding. Further molecular dynamics experiments found that binding of heparin occurred at the sulfates and glucosamines in heparin. Phosphate ions could interact with the heparin via sodium ions to impair the MB-heparin binding. Finally, our model found 3.7-fold more MB dimerization upon addition of heparin in MB solution confirming that heparin facilitates MB aggregation. We conclude that the addition of heparin in MB *decreases* the absorbance of the sample because of MB–heparin aggregation leading to fewer MB molecules in solution; however, the aggregation also *increases* the PA intensity because the MB molecules in the MB–heparin aggregate have reduced degrees of freedom and poor heat transfer to solvent.

Graphical Abstract

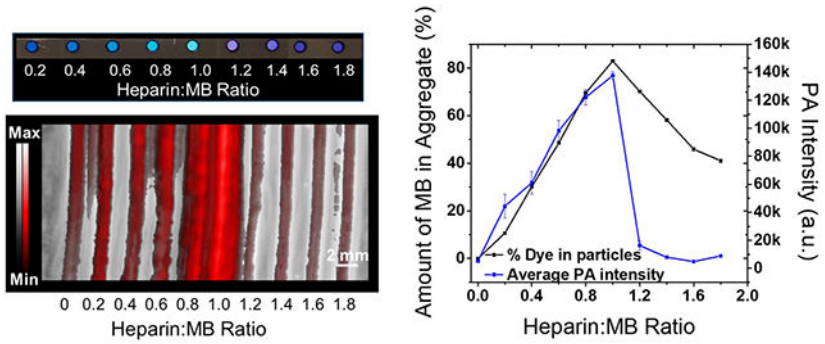

INTRODUCTION

Methylene blue (MB) is a phenothiazinium dye with diverse biomedical applications. It is a photosensitizer used in photodynamic therapy and as a contrast agent in photoacoustic (PA) imaging.[1-8] Moreover, MB is US Food & Drug Administration-approved for managing methemoglobinemia[9] and can treat malaria.[10]

MB has also been used in monitoring heparin.[11-13] Heparin is a highly sulfated anionic glycosaminoglycan that activates antithrombin, which silences the clotting factors thrombin and Factor Xa.[14] Intriguingly, mixing heparin and MB decreases the MB absorption[15] and increases the resonant Rayleigh scattering[16] of MB; thus, MB can monitor heparin. MB can also measure heparin electrochemically because heparin reduces the peak current of MB in cyclic voltammetry.[11] More recently, we reported a real-time PA method to monitor heparin in blood using MB—the PA intensity of MB significantly increased upon the addition of heparin.[13] In PA imaging, the signal is proportional to absorption;[17-19] however, we were surprised to find that the absorbance of MB decreased with increasing heparin dose yet the PA signal increased—this is in contrast to most other “turn on” PA probes whereby increased absorption facilitates increased PA signal. That observation motivates this work.

Mechanistic studies of the MB/heparin interaction are rare and mainly limited to spectroscopic studies in water. Previous research found that 610 and 660 nm are characteristic peaks of the MB dimer and monomer, respectively.[20] Upon addition of heparin, the absorbance of MB shifted from 660 to 610 and eventually to 570 nm, which indicated the formation of MB dimers and MB self-aggregates (i.e., H-type aggregates).[21,22]

This shift is caused by the coupling between MB molecules that splits an excited singlet state of MB into two excitonic states. The absorption from ground state and to upper excitonic state blue-shifts the absorbance spectrum.[23,24] However, these studies lacked deeper mechanistic detail and only investigated the interaction in water, which disregards the key role of pH and ionic strength—our interest lies in measuring heparin with PA in whole blood and motivates this mechanistic study of the interaction between heparin and MB in more biologically relevant solvents.

Here, we describe MB–heparin interactions in water and phosphate buffer saline (PBS) including the identification of MB–heparin aggregation. We found that formation of MB–heparin aggregate was responsible for the absorbance reduction and PA enhancement of MB upon addition of heparin. PBS could impair the MB–heparin binding by shielding the MB and heparin. We also include simulation results that further detail the heparin binding residues and identify the intramolecular interactions that stabilized the MB–heparin aggregation.

RESULTS AND DISCUSSION

We used nuclear magnetic resonance (NMR), dynamic light scattering (DLS), and optical absorbance spectroscopy to study the binding between heparin and MB as well as the change in the PA signal. We then characterized the impact of PBS and solvent ionic strength on the binding and finally performed molecular simulations to support the experimental observations.

MB–Heparin Aggregation Induces PA Enhancement.

The PA enhancement of MB in the presence of heparin reverses when heparin is above a certain concentration.[13] Therefore, we hypothesize that MB electrostatically binds to heparin, and the binding kinetics varies as a function of heparin concentration. Heparin is a highly sulfated and negatively charged polysaccharide, and thus we estimate the number of sulfate groups on heparin for MB binding to characterize the effect of heparin concentration as follows: Heparin has an antithrombin binding pentasaccharide site as minor repeat units and two trisulfated disaccharide units as major repeat units in its backbone[25] (Figure S1). The molecular weight of commercial heparin varies, but the number of sulfate in heparin can be estimated via the number of the major trisulfated disaccharide repeat units. Each major repeat unit has 3 sulfate groups for 3 MB molecules to bind with, and the molecular weight of each repeat unit is 591.4 g/mol, which is used to estimate the number of sulfate group of heparin per unit weight. To study the effect of heparin concentration on PA signal, we prepared 0.90 mg/mL MB and varied the amount of heparin in the MB solution from 0.09 to 0.85 mg/mL. Thus, the ratio of MB to the sulfate groups on heparin was 1:0.2–1:1.8.

We studied these samples with NMR. The chemical shift and relaxation time of MB are sensitive to the microenvironment and distance between MB molecules. Therefore, the NMR spectra of aqueous solutions containing different ratios of heparin to MB were studied to characterize the binding of MB to heparin. First, the MB concentration was optimized to 0.9 mg/mL to achieve sufficient signal-to-noise ratio in ^{1}H NMR. MB is a positively charged dye and has three types of aromatic protons at the phenothiazinium central ring and two sets

of identical protons at the dimethylamino groups corresponding to 7.40, 7.11, 6.87, and 3.14 ppm in the NMR spectrum (Figure 1A inset).[26,27] Proton 1 changed the most upon addition of heparin. The NMR signal at 7.40 ppm decreased by 75.7% with a downshift of 0.1 ppm when the heparin:MB ratio increased from 0.2 to 1.0 (Figure 1A). The decrease in NMR intensity suggested precipitation of the MB–heparin aggregates because the protons of MB sequestered in the aggregates should have reduced NMR signal due to concentration quenching.[27]

DLS analysis revealed that the size of MB–heparin aggregate increased as a function of MB concentration. At a constant heparin concentration (0.00625 mg/mL), increasing the MB:heparin ratio from 0.31 to 0.93 increased the size of the MB–heparin aggregate by 4.9-fold (Figure 1B). However, increasing the heparin:MB ratio from 0.08 to 0.64 had only 1.5-fold increase on the aggregate size (Figure S2). The more significant increase governed by the MB concentration than the heparin concentration suggests that the MB–heparin aggregation and precipitation results from charge neutralization between MB and heparin and interactions between MB molecules such dimerization that could facilitate aggregation of different MB-bound heparins.

The absorbance of samples with 0.9 mg/mL MB with heparin to MB ratio from 0.2 to 1.8 were found to correlate with the amount of MB in the MB–heparin aggregates. Despite a constant MB concentration across all mixtures, the absorbance of MB at 660 and 610 nm decreased 4.0-fold and 4.5-fold when heparin:MB was equal to 1.0:1.0 (Figure 1C), respectively. Concurrently, 85% of the MB was sequestered in the MB–heparin aggregates at heparin to MB ratio of 1.0 (Figure 1D). This indicated that the decrease of absorbance at the 610 and 660 nm was a result of MB–heparin aggregation that decreased the amount of free MB dimer and monomers and therefore the absorbance in the solution.

Higher heparin concentrations beyond a 1:1 ratio of heparin to MB led to MB *self*-aggregation rather than MB–heparin aggregation as indicated by the absorbance peak at 570 nm.[22] Meanwhile, the amount of MB in the MB–heparin aggregates decreased by 2.0-fold (Figure 1F). The initial color change of MB at heparin:MB ratio below 1.0 as well as the reversal at heparin:MB over 1.0 also indicate the aggregation and dispersion of MB–heparin (Figure 1D). This is analogous to the precipitation of other dyes such as rhodamine 6G in aqueous sodium dodecyl sulfate.[28] The dispersion of MB–heparin aggregate was likely due to the electrostatic repulsion between the heparin chains. Therefore, MB neutralized heparin and formed MB–heparin aggregates when the heparin:MB ratio was between 0 and 1.0. Higher doses of heparin dispersed the MB–heparin aggregates likely because of the electrostatic repulsion between negative heparin chains.

The PA enhancement of the MB–heparin mixture was also a function of heparin to MB ratio. The PA intensity of the MB at heparin:MB ratio of 1.0 measured at 680 nm was 26.7-fold higher than MB alone, but it decreased 15.6-fold when the heparin:MB ratio was 1.8 (Figure 1D and F). This was very similar to the trend seen for the amount of MB in the MB–heparin aggregates (Figure 1F). We also found that the MB–heparin aggregates contributed most of the PA intensity of the MB–heparin mixtures. We separated the aggregates and soluble fractions and found that the PA intensity of the precipitate was 43.1-fold higher than the

supernatant suggesting that the PA enhancement was a result of MB–heparin aggregation (Figure 1E). Therefore, the formation of MB–heparin aggregates contributes to the photoacoustic increase. The enhanced PA intensity caused by the MB–heparin aggregation was likely a result of the reduced degrees of freedom of the MB (its molecular motions are restricted relative to free MB). This led to poor heat transfer from the aggregate to the solvent and increased the thermal gradient between the aggregate and solution.[29]

Impact of PBS.—Next, we prepared the MB–heparin samples in PBS using heparin:MB ratio of 0.8 and 1.8 to study the impact of PBS on MB–heparin aggregation and MB self-aggregation. At a heparin:MB ratio of 0.8 and MB concentration at 0.15 mM, PBS had minimal influence on absorption wavelength but increased the absorbance by 24% and 9% at 610 and 660 nm, respectively, compared to the MB–heparin sample in water (Figure 2A Hep:MB = 0.8 in water and Hep:MB = 0.8 1 × PBS). This led to a 22% PA increase at 680 nm excitation (Figure 2B 0.8 H_2O and 0.8 PBS). PBS had an even more pronounced impact at heparin:MB of 1.8 (MB still at 0.15 mM): PBS red-shifted the absorbance of the sample from 570 to 610 nm (Figure 2A Heparin:MB = 1.8 1 × PBS) indicating disassociation of MB self-aggregates to MB dimer. The PBS also increased the PA intensity of the sample by 2.8-fold (Figure 2B 1.8 PBS). We hypothesized that this spectral shift and PA enhancement was due to the ionic strength rather than the pH of the PBS.

To test this hypothesis, we performed a control experiment using 137 mM NaCl because PBS contains 137 mM NaCl and is much more concentrated than other buffer ions (i.e., 13.7 times higher than phosphate buffer and 50.7 times higher than potassium chloride). Adding 137 mM NaCl reversed the absorbance of MB–heparin mixture in water from 570 to 610 nm with a spectral profile very similar to the effect of adding 1 × PBS (Figure 2A Hep:MB = 1.8 137 mM NaCl). To further verify that the ionic strength is responsible for the spectral shift, we increased the MB concentration to 2.4 mM and maintained the heparin:MB ratio at 1.0—it should take more PBS and NaCl to shift the absorbance from 570 to 610 nm. Indeed, we had to double the PBS or NaCl concentration to completely shift the absorbance of the sample from 570 to 610 nm (Figure 2C). This result suggests that the ions in PBS can disassociate the MB self-aggregate via ionic shielding leading to an absorbance redshift.

We further tested the influence of ionic strength on PA intensity of MB–heparin mixture at a heparin:MB ratio of 1.8 using 137 mM NaCl. The addition of 137 mM NaCl in the MB–heparin sample had a 2.0-fold higher PA signal than the sample in water (Figure 2B 1.8 NaCl) and increased the number of aggregates. Compared to the MB–heparin sample with heparin:MB at 0.8, the sample with heparin:MB ratio at 1.8 has more heparin that uses more NaCl as counterions—this minimizes the shielding effect and leads to more heparin-MB aggregates.

Molecular Modeling of MB–Heparin Binding.

Finally, we used molecular modeling to study the binding details of MB and heparin (repeat unit used in the simulation shown in Figure 3A) as well as the role of heparin in MB self-aggregation. To study the impact of PBS in the MB–heparin binding, simulations were first performed using 0.154 M NaCl without phosphate ions to balance the charge of MB and

heparin. The binding process of MB and heparin were dynamic in both 0.154 M NaCl and 1X PBS with rapid association and dissociation of the MB with heparin (Video 1 and Video 2 for NaCl and PBS, respectively). We found that the PBS ions shielded MB and the heparin because phosphates associated with heparin via multiple Na^+(Figure S4).

We also compared the number of MB dimers formed between the system with MB alone and the system with MB and heparin. Dimer formation was defined as a distance of less than 4.8 Å between the centers of mass between two MB molecules. Dimer formation for three trials of the system containing 14 MB molecules with and without heparin present were analyzed. The addition of heparin increased MB dimer formation by 3.7-fold compared to MB alone ($p < 0.03$, Figure 3B). All other variables, including the placement of MB within the solvation box, were kept constant. These results suggested that the presence of heparin increases the frequency of MB dimer formation and facilitates MB–heparin aggregation.

We also studied the mechanism by which MB dimer formation depends on heparin. This analysis aimed to determine if π–π interactions were a plausible explanation for dimer formation. We defined a MB–MB binding event as a distance less than 9.5 Å between the center of mass of MB molecules because this distance is the length of MB from terminal C to terminal C and accounts for all angles of MB binding other than a perpendicular binding event (no perpendicular events were noted in any of the simulations). The frequency of binding events at 9.5 Å was compared to the frequency of binding events at 4.0 Å, which is the widely accepted upper limit of π–π interactions[30] (Figure 3C). This comparison revealed that of the dimers that were formed without heparin, only 17.6% had an orientation and distance indicative of a π–π interaction (Figure 3D). With heparin, 31.3% of the dimers had an orientation and distance suggestive of π–π interactions. These differences were statistically significant ($p < 0.01$), and this result indicates that heparin enhances MB π–π stacking to facilitate MB precipitation into the MB–heparin aggregate.

To understand the heparin binding sites, we evaluated each monosaccharide unit in the simulated heparin structure for its energetic contribution to a MB binding event using Molecular Mechanics–Poisson–Boltzmann Surface Area (MMPBSA) decomposition analysis.[31] Figure 4A showed that the spontaneity of a binding event was mostly due to the glucosamine (GlcN) and sulfate groups; thus, these residues were likely stable MB binding sites. The sulfate groups were distributed throughout the structure and underlie the anionic nature of heparin, and they strongly contributed to the overall energetics of a MB binding event. The interaction between MB and binding residues in heparin are electrostatic (Figure 4B), and this electrostatic interaction neutralizes the charge of both the heparin residue and MB upon binding.

CONCLUSIONS

In summary, we studied the binding of MB and heparin in experiments and simulations. In water, MB aggregates with heparin via charge neutralization, resulting in MB sequestration in these aggregates. Therefore, the MB–heparin aggregation reduces the absorbance of the sample because there are fewer MB molecules in solution; however, this aggregation also *increases* the PA intensity because the MB molecules in the MB–heparin aggregate have

reduced degrees of freedom and poor heat transfer to the solvent. Higher heparin concentrations disperse the MB–heparin aggregate because of the electrostatic repulsion between heparin chains—this forms MB-self-aggregates. PBS can disassociate the MB self-aggregates into dimers because of the ionic shielding of chloride ions. Decomposition analysis indicated that the stable binding sites were the sulfate groups and the glucosamine groups of the heparin. The addition of heparin to MB increases the frequency of MB dimer formation. A significant portion of dimers had an orientation suggestive of π–π stacking. These trends confirmed our experimental observation that MB neutralized by heparin tended to aggregate via π–π stacking.

MATERIALS AND METHODS

Reagents.

MB (98%) and PBS tablets were purchased from Fisher. Dissolving one PBS tablet in 200 mL deionized water should result in 0.01 M phosphate buffer, 0.0027 M potassium chloride, 0.137 M NaCl, and pH 7.4 at 25 °C. Heparin sodium salt from porcine intestinal mucosa (grade I-A, ≥ 180 U/mg) and protamine sulfate salt from salmon were purchased from Sigma. Heparin (sodium injection, 1000 United States Pharmacopeia (USP) U/mL) was purchased from SAGENT pharmaceuticals. Deuterium oxide (D, 99.9%) was purchased from Cambrige Isotope Laboratories, Inc. Enoxaparin sodium (LMWH) injection was purchased from Winthrop. Laboratory polyethylene tubing (OD: 1.27 mm, ID: 0.85 mm) was purchased from Harvard Apparatus.

Preparation of MB–Heparin Mixtures.

Stock MB solution MB was prepared by dissolving 1.898 mM MB in (M.W., 373.90 g/mol) deuterated water (D_2O) with sonication at 40 °C for 30 min. The final MB concentration was 4.8 mM. The molecular weight of the trisulfated disaccharide repeat units in heparin backbone was 591.4 g/mol.[32] The final heparin concentration was tuned based on the sulfate equivalence to get a 0, 0.2, 0.4, 0.6, 0.8, 1.0, 1.2, 1.4, 1.6, and 2.0 equivalence of heparin with respect to MB (final concentration of 2.4 mM). This was accomplished by mixing 0.6 mL of 4.8 mM MB solution with 0 to 540 μL of 1.898 mg/ mL heparin solution. Additional D_2O was added into the sample to keep the total volume at 1.2 mL.

To characterize the influence of MB on the aggregate size, 500 μL of 0.2, 0.3, 0.4, and 0.6 mM MB was added into 500 μL of 0.0125 mg/mL heparin solution. The influence of heparin concentration on the MB–heparin aggregate size was measured by mixing 500 μL of 0.4 mM MB with 500 μL of 0.0625, 0.125, 0.25, and 0.5 mg/mL heparin.

To study the effect of PBS, PBS tablet was crushed into powders. MB–heparin sample with 2.4 mM MB and 1 × PBS was prepared by mixing 0.6 mL of 1.8 mg/mL (i.e., 4.8 mM) MB solution with 0.6 mL heparin (0.94 mg/mL for heparin:MB ratio at 1.0 or 1.70 mg/mL for heparin:MB ratio at 1.8) that contains 12 mg PBS powder. In the sample with 2 × PBS, the amount of PBS was increased to 24 mg. MB–heparin sample with 0.15 mM MB and 1 × PBS was prepared by mixing 0.6 mL 0.1125 mg/mL (i.e., 0.3 mM) MB with 0.6 mL heparin (0.047 mg/mL for heparin:MB ratio at 0.8 and 0.106 mg/mL for heparin:MB ratio at 1.8)

that contains 12 mg PBS powder. The influence of NaCl was characterized by dissolving 9.6 (i.e., 137 mM) or 19.2 (i.e., 274 mM) mg NaCl powder in the MB–heparin solution.

NMR Characterization.

The NMR spectra of 2.4 mM MB with 0.2, 0.4, 0.6, 0.8, 1.0, 1.4, and 1.8 equivalence of heparin were measured using a Bruker AVA 300 MHz NMR spectrometer to study the aggregation of MB in the presence of heparin. The number of scans used was kept constant at 32 scans to compare the NMR peak intensity between different mixtures.

Characterization Using Absorbance Spectroscopy.

The solutions were mixed by vertexing and transferred into a 4 μL well plates for absorbance measurement. The amount of dye sequestered in the MB–heparin aggregates was estimated by measuring the absorbance of the supernatant of the samples that had been centrifuged at 10 000 rpm for 5 min. Then the area under the peak between 400 and 800 nm was used to calculate the relative amounts of MB sequestered in the precipitate formed after addition of heparin. All absorbance spectra were measured by SpectraMax M5 spectrophotometer.

PA Characterization.

About 17 μL of MB-heparin mixtures used for absorbance and NMR studies were transferred into the polyethylene tubing. The PA image of these tubes were acquired on PA imaging system (Visualsonics) with analysis and parameters described previously.[13] The 3D images acquired were processed using ImageJ software to estimate the pixel intensities.[33]

Computational Methodology.

The structure of heparin was constructed via GLYCAM Carbohydrate Builder software.[34] Specifically, the four monosaccharide units that were used in this study were YZB, WYS, YuA, and QYS. This pattern was repeated six times to construct the heparin polysaccharide. Each monosaccharide and MB was parametrized using Gaussian HF/6-31G*[35] through the WebMO interface.[36] The surface of heparin was evaluated as a potential binding surface for MB using the VMD software.[37] MB was docked to heparin using AutoDock Vina[38] placing MB within each of the possible binding sites, then simulating only the 14 most favorable docking conformations.

Heparin–MB interactions were characterized *in silico* using molecular dynamics simulations. Simulations were performed on heparin with 0, 1, 4, 7, 10, and 14 MB docked in the presence of either a PBS solvent system or a 0.154 M NaCl solvent system that closely reflected experimental conditions. The simulation of the 0.154 M NaCl and PBS systems were performed in six MB concentrations (0, 1, 4, 7, 10, 14 MBs) for 3 trials per concentration, resulting in 36 systems. Each system was minimized in seven restrained steps to eliminate bad contacts, heated in one step to 300 K, and equilibrated in seven steps, with each step reducing the imposed restraints on the systems. These preparatory operations and the unrestrained simulations were all completed using Amber 16[39] with the *ff14SB*[40] and GAFF force fields,[41] while also utilizing additional parameters provided by GLYCAM. All unrestrained simulations were run for a minimum of 100 ns, with a time step of 2 fs, and at constant temperature and pressure of 300 K and 1 atm, respectively. Binding events of MB

to heparin were measured using a 9.47 Å distance between the center of mass of MB and the nearest heparin residue. We evaluated the frequency of dimer formation per every 10 ns of simulated time. A dimer that could have π–π interactions was defined as a distance of less than 4.0 Å between the two centers of mass. Visualization and distance analyses were completed using VMD and the *cpptraj* module of Amber, respectively.[42] Free energy analysis was performed on each simulation using the MMPBSA.py[31] module of Amber.

Data Analysis and Statistical Treatment.

The average and standard deviation of the integrated density were calculated using Microsoft excel functions “AVERAGE” and “STDEV”. *P* value of the number of MB dimer formation was calculated via the one-tailed test using Microsoft Excel functions “TTest”.

Supplementary Material

Refer to Web version on PubMed Central for supplementary material.

ACKNOWLEDGMENTS

We acknowledge funding from NIH: DP2 HL137187, R00 HL117048, and infrastructure from S10 OD021821. Computational resources were provided in part by the MERCURY consortium under NSF grants CHE-1229354 and CHE-1662030.

REFERENCES

(1). Acosta-Avalos D, Jedlicka LDL, Costa MS, Barja PR, and da Silva EC (2012) Photoacoustic spectroscopy of *Candida albicans* treated with methylene blue. Int. J. Thermophys 33, 1864–1869.

(2). Erpelding TN, Kim C, Pramanik M, Jankovic L, Maslov K, Guo Z, Margenthaler JA, Pashley MD, and Wang LV (2010) Sentinel lymph nodes in the rat: noninvasive photoacoustic and US imaging with a clinical US system. Radiology 256, 102–110. [PubMed: 20574088]

(3). Tang W, Xu H, Kopelman R, and Philbert MA (2005) Photodynamic characterization and *in vitro* application of methylene blue-containing nanoparticle platforms. Photochem. Photobiol 81, 242–249. [PubMed: 15595888]

(4). He X, Wu X, Wang K, Shi B, and Hai L (2009) Methylene blue-encapsulated phosphonate-terminated silica nanoparticles for simultaneous in vivo imaging and photodynamic therapy. Biomaterials 30, 5601–5609. [PubMed: 19595455]

(5). Tardivo JP, Del Giglio A, de Oliveira CS, Gabrielli DS, Junqueira HC, Tada DB, Severino D, de Fátima Turchiello R, and Baptista MS (2005) Methylene blue in photodynamic therapy: From basic mechanisms to clinical applications. Photodiagn. Photodyn. Ther 2, 175–191.

(6). Hariri A, Lemaster J, Wang J, Jeevarathinam AS, Chao DL, and Jokerst JV (2018) The characterization of an economic and portable LED-based photoacoustic imaging system to facilitate molecular imaging. Photoacoustics 9, 10–20. [PubMed: 29234601]

(7). Wang J, Lin C-Y, Moore C, Jhunjhunwala A, and Jokerst JV (2018) Switchable photoacoustic intensity of methylene blue via sodium dodecyl sulfate micellization. Langmuir 34, 359–365. [PubMed: 29232146]

(8). Bohndiek SE, Sasportas LS, Machtaler S, Jokerst JV, Hori S, and Gambhir SS (2015) Photoacoustic tomography detects early vessel regression and normalization during ovarian tumor response to the antiangiogenic therapy trebananib. J. Nucl. Med 56, 1942–1947. [PubMed: 26315834]

(9). Clifton JI, and Leikin JB (2003) Methylene Blue. American Journal of Therapeutics 10, 289–291. [PubMed: 12845393]

(10). Schirmer RH, Coulibaly B, Stich A, Scheiwein M, Merkle H, Eubel J, Becker K, Becher H, Muller O, Zich T, et al. (2003) Methylene blue as an antimalarial agent. Redox Rep. 8, 272–275. [PubMed: 14962363]

(11). Tan L, Yao S, and Xie Q (2007) Electrochemical determination of heparin using methylene blue probe and study on competition of Ba2+ with methylene blue for binding heparin. Talanta 71, 827–832. [PubMed: 19071381]

(12). Němcová I, Rychlovský P, Havelcová M, and Brabcová M (1999) Determination of heparin using flow injection analysis with spectrophotometric detection. Anal. Chim. Acta 401 , 223–228.

(13). Wang J, Chen F, Arconada-Alvarez SJ, Hartanto J, Yap L-P, Park R, Wang F, Vorobyova I, Dagliyan G, Conti PS, et al. (2016) A Nanoscale tool for photoacoustic-based measurements of clotting time and therapeutic drug monitoring of heparin. Nano Lett. 16, 6265–6271. [PubMed: 27668964]

(14). Jin L, Abrahams JP, Skinner R, Petitou M, Pike RN, and Carrell RW (1997) The anticoagulant activation of antithrombin by heparin. Proc. Natl. Acad. Sci. U. S. A 94, 14683–14688. [PubMed: 9405673]

(15). Jiao Q, and Liu Q (1999) Characterization of the interaction between methylene blue and glycosaminoglycans. Spectrochim. Acta, Part A 55, 1667–1673.

(16). Luo HQ, Liu SP, Liu ZF, Liu Q, and Li NB (2001) Resonance Rayleigh scattering spectra for studying the interaction of heparin with some basic phenothiazine dyes and their analytical applications. Anal. Chim. Acta 449, 261–270.

(17). Cox B, Laufer J, and Beard P (2009) Proc. SPIE, 717713.

(18). Gupta S, Chatni MR, Rao ALN, Vullev VI, Wang LV, and Anvari B (2013) Virus-mimicking nano-constructs as a contrast agent for near infrared photoacoustic imaging. Nanoscale 5, 1772–1776. [PubMed: 23334567]

(19). Kim T, Lemaster JE, Chen F, Li J, and Jokerst JV (2017) Photoacoustic imaging of human mesenchymal stem cells labeled with Prussian Blue–poly(l-lysine) nanocomplexes. ACS Nano 11, 9022–9032. [PubMed: 28759195]

(20). Rabinowitch E, and Epstein LF (1941) Polymerization of dyestuffs in solution. thionine and methylene blue. J. Am. Chem. Soc 63, 69–78.

(21). Liu Q, and Jiao Q (1998) Mechanism of methylene blue action and interference in the heparin assay. Spectrosc. Lett 31, 913–924.

(22). Braswell E (1968) Evidence for trimerization in aqueous solutions of methylene blue. J. Phys. Chem 72, 2477–2483.

(23). Severino D, Junqueira HC, Gugliotti M, Gabrielli DS, and Baptista MS (2003) Influence of negatively charged interfaces on the ground and excited state properties of methylene blue. Photochem. Photobiol 77, 459–468. [PubMed: 12812286]

(24). Morgounova E, Shao Q, Hackel BJ, Thomas DD, and Ashkenazi S (2013) Photoacoustic lifetime contrast between methylene blue monomers and self-quenched dimers as a model for dual-labeled activatable probes. J. Biomed. Opt 18, 056004–056004.

(25). Casu B, Naggi A, and Torri G (2015) Re-visiting the structure of heparin. Carbohydr. Res 403, 60–68. [PubMed: 25088334]

(26). Sueishi Y, Inazumi N, and Hanaya T (2005) Effects of pressure on inclusion complexation of methylene blue with watersoluble p-sulfonatocalix[n]arenes. J. Phys. Org. Chem 18, 448–455.

(27). Moreno-Villoslada I, Torres C, González F, Shibue T, and Nishide H (2009) Binding of methylene blue to polyelectrolytes containing sulfonate groups. Macromol. Chem. Phys 210, 1167–1175.

(28). Micheau J, Zakharova G, and Chibisov A (2004) Reversible aggregation, precipitation and re-dissolution of rhodamine 6G in aqueous sodium dodecyl sulfate. Phys. Chem. Chem. Phys 6, 2420–2425.

(29). Chen Y-S, Yoon SJ, Frey W, Dockery M, and Emelianov S (2017) Dynamic contrast-enhanced photoacoustic imaging using photothermal stimuli-responsive composite nanomodulators. Nat. Commun 8, 15782. [PubMed: 28593942]

(30). McGaughey GB, Gagné M, and Rappé AK (1998) π-Stacking interactions alive and well in proteins. J. Biol. Chem 273, 15458–15463. [PubMed: 9624131]

(31). Miller BR III, McGee TD Jr, Swails JM, Homeyer N, Gohlke H, and Roitberg AE (2012) MMPBSA.py: an efficient program for end-state free energy calculations. J. Chem. Theory Comput 8, 3314–3321. [PubMed: 26605738]

(32). Shriver Z, Capila I, Venkataraman G, and Sasisekharan R (2012) Heparin and heparan sulfate: analyzing structure and microheterogeneity. In Handbook of Experimental Pharmacology, pp 159–176. [PubMed: 22566225]

(33). Abràmoff MD, Magalhães PJ, and Ram SJ (2004) Image processing with ImageJ. Biophotonics Int. 11, 36–42.

(34). Woods R (2005) GLYCAM-Web. Complex Carbohydrate Research Center, University of Georgia, Athens, GA.

(35). Frisch MJ, Trucks GW, Schlegel HB, Scuseria GE, Robb MA, Cheeseman JR, Scalmani G, Barone V, Petersson GA, and Nakatsuji H, et al. (2016) Gaussian 16, Revision B.01.

(36). WebMO Enterprise 14.0.006e, WebMO LLC, Holland, MI, 2011.

(37). Humphrey W, Dalke A, and Schulten K (1996) VMD: visual molecular dynamics. J. Mol. Graphics 14, 33–38.

(38). Trott O, and Olson AJ (2009) AutoDock Vina: improving the speed and accuracy of docking with a new scoring function, efficient optimization, and multithreading. J. Comput. Chem 31, 455–461.

(39). Case DA, Cerutti DS, Cheatham TE, Darden TA III, Duke RE, Giese TJ, Gohlke H, Goetz AW, Greene D, and Homeyer N, et al. (2017) AMBER 2017. University of California, San Francisco.

(40). Maier JA, Martinez C, Kasavajhala K, Wickstrom L, Hauser KE, and Simmerling C (2015) ff14SB: Improving the accuracy of protein side chain and backbone parameters from ff99SB. J. Chem. Theory Comput 11, 3696–3713. [PubMed: 26574453]

(41). Wang J, Wolf RM, Caldwell JW, Kollman PA, and Case DA (2004) Development and testing of a general amber force field. J. Comput. Chem 25, 1157–1174. [PubMed: 15116359]

(42). Roe DR, and Cheatham TE III (2013) PTRAJ and CPPTRAJ: software for processing and analysis of molecular dynamics trajectory data. J. Chem. Theory Comput 9, 3084–3095. [PubMed: 26583988]

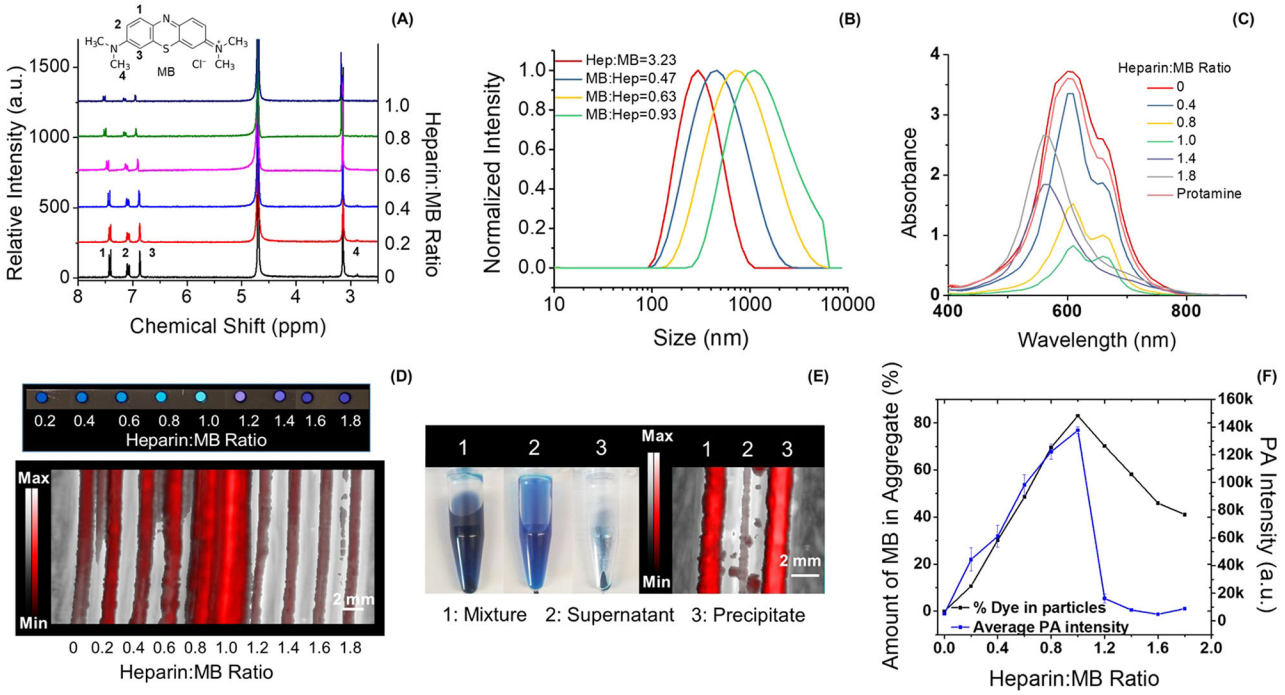

Figure 1.

MB aggregation upon addition of heparin. Panel A plots the NMR spectra of MB at the heparin:MB ratios of 0 to 1.0. Peaks 1, 2, 3, and 4 in the spectrum correspond to the protons shown on the structure of MB (inset). The NMR intensity of both proton 1 and proton 4 (Figure S3) decreased the most (i.e., 76%) when the heparin:MB ratio approaches 1.0, suggesting the precipitation of MB–heparin aggregates. Panel B shows the DLS result of MB–heparin aggregates as a function of MB concentration. The size of the aggregates increased from 335 to 1632 nm when the MB:heparin ratio increased from 0.31 to 0.93. The absorbance spectra of the samples in panel A are shown in panel C. The absorbance intensity at 610 nm decreased 4.5-fold when heparin:MB ratio equals 1.0. A higher heparin:MB ratio from 1.2–1.8 blue-shifts the absorbance peak to 570 nm suggesting the formation of MB self-aggregates (i.e., H-type aggregates). A control experiment using 0.95 mg/mL protamine (i.e., antagonist of heparin) reverses the spectral change. Panel D shows the color and PA image of the samples of panel C. In the sample with heparin:MB at 1.0, the MB–heparin aggregates were collected by centrifugation—these aggregates cause most of the PA signal in the mixture (panel E). Panel F quantifies the PA intensity of the samples in panel D and the amount of MB in the MB–heparin aggregates. The similar trend indicates that the MB–heparin aggregation increases PA intensity. The error bars in panel F represent the standard deviation of 8 regions-of-interest in the sample.

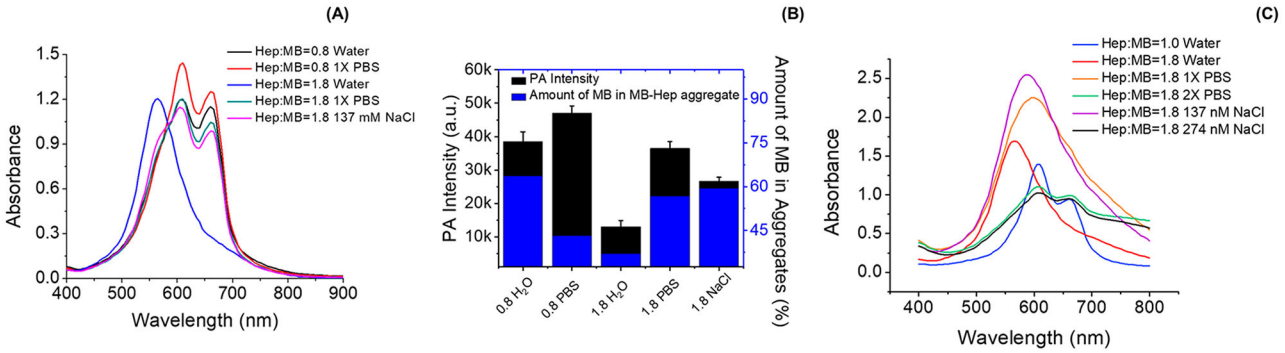

Figure 2.

Impact of PBS in the MB–heparin binding. Panel A compares the spectral change of MB–heparin complex in water and PBS. The MB–heparin sample with heparin:MB at 0.8 in PBS (red) had 24% and 9% higher absorbance at 610 and 660 nm than the sample prepared in water (black). The addition of 1xPBS to a mixture with heparin:MB of 1.8 in water (blue) shifted the absorbance from 570 nm to 610 nm (green). A similar effect was observed upon the addition of 137 mM NaCl (purple) Panel B shows the PA intensity (black) and the amount of MB in the MB–heparin aggregates (blue) of the samples in Panel A. At heparin:MB of 0.8, PBS (0.8 PBS) increased the PA signal of the sample in water (0.8 H_2O) by 22%. At heparin:MB of 1.8, adding PBS (1.8 PBS) and 137 mM NaCl (1.8 NaCl) in the sample prepared in water (1.8 H_2O) resulted in 2.8- and 2.0-fold increase in PA intensity as well as 1.5- and 1.6-fold in the amount of MB in MB–heparin aggregate. Panel C is the absorbance of 2.4 mM MB with heparin:MB ratio at 1.0 (blue) and 1.8 (red). Adding 1 × PBS (orange) or 137 mM NaCl (purple) only red-shifted the absorbance to 590 and 600 nm. Doubling the PBS (green) or NaCl concentration (black) in the sample could shift the absorbance to 610 nm, like the absorbance of sample with Heparin:MB ratio at 1.0. This indicates that the ionic strength governs the disassociation of MB self-aggregates to MB dimer.

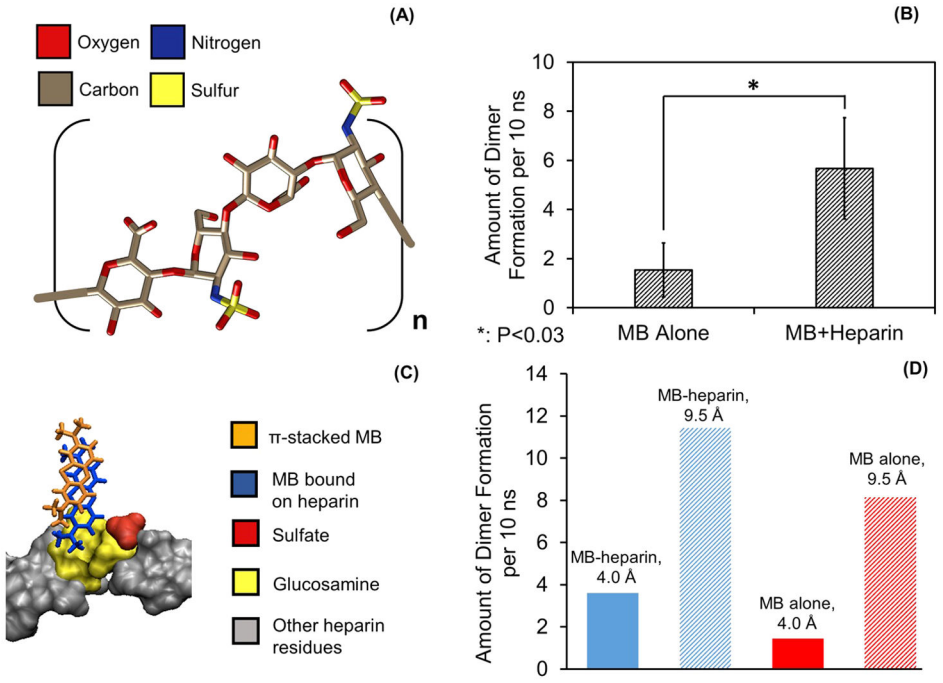

Figure 3.

Simulated binding kinetics of MB and heparin. Panel A shows one of the 6 repeating units of heparin simulated in solvent NaCl and PBS systems. Panel B shows that the MB system with heparin had on average 5.67 ± 2.06 dimer formations per 10 ns, which is significantly more MB dimer formation than the system without heparin (1.53 ± 1.10 dimer formations per 10 ns ($p < 0.03$)). Panel C shows the π–π stacked MB dimer bound on the sulfate and glucosamine. The fraction of MB dimers formed by π–π stacking (distance between two MB molecules was less than 4.0 Å) among the total number of MB dimers (distance between two MB molecules was less than 9.5 Å) is shown in panel D. In the pure MB system, the π–π stacked MB dimer is 17.6% of the total dimers. The percentage increased to 31.3% upon addition of heparin. Error bars in B represent three replicate simulations runs.

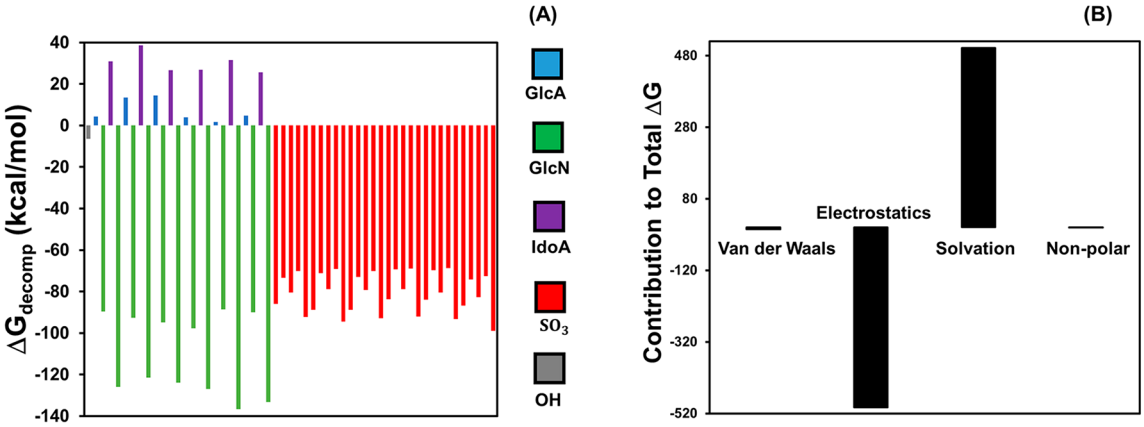

Figure 4.

Decomposition analysis of the binding energy. The energy decomposition results of heparin residues in the system of 7 MB molecules with 1 heparin are plotted in panel A. Here, positive values indicate a destabilizing effect, and negative values represent stabilizing residues with respect to a binding event. The glucosamine and sulfate residues were the largest contributors to the spontaneity of the MB binding event. The GlcA, GlcN, IdoA, SO_3, and OH represent glucuronic acid, glucosamine, iduronic acid, sulfate, and the hydroxide terminals that are not associated with other residues, respectively. The X-axis represents different residues on the heparin. These monosaccharides are presented in the order that they appear in the polysaccharide; the sulfates are presented as a group although they are scattered throughout the structure. Panel B further details the energetic contributions of van der Waals forces, electrostatic interactions, the solvation free energy upon binding of the ligand to the receptor, and the nonpolar contribution of the surface, respectively. Electrostatic interactions were the greatest stabilizing force to the energetics of binding, while solvation effects were found to be the most destabilizing force.